Applications of Inertial-Sensor High-Inheritance Instruments to DSN Precision Antenna Pointing

R. E. Goddard
Guidance and Control Section

Laboratory test results of the initialization and tracking performance of an existing inertial-sensor-based instrument are given. The instrument, although not primarily designed for precision antenna pointing applications, demonstrated an on-average 10-hour tracking error of several millidegrees. The system-level instrument performance is shown by analysis to be sensor limited. Simulated instrument improvements show a tracking error of less than 1 mdeg, which would provide acceptable performance, i.e., low pointing loss, for the DSN 70-m antenna subnetwork, operating at Ka-band (1-cm wavelength).

I. Introduction

Inertial sensors provide data on acceleration and spin vectors with respect to a stationary frame of reference. These data are processed by a strap-down instrument to provide the pointing coordinates of a large-structure antenna. The strap-down instrument is retrofit onto the primary reflector of the large-structure antenna, thus bypassing many error sources, such as gimbal encoders,[1] azimuth plane tilt, axis misalignments, and the Master Equatorial System.[2] A high-inheritance instrument is an existing instrument with minor modifications. Utilization of high-inheritance instruments yields cost savings in design, analysis, manufacturing, and test. In this article, the pointing performance of an inertial-sensor-based high-inheritance instrument is given. The inertial instrument is a navigator, capable of providing attitude (e.g., azimuth and elevation antenna coordinates) from the output of a triad of ring laser gyroscopes and accelerometers [1,2]. As a reference to antenna pointing requirements, the DSN 70-m antenna at Ka-band (1-cm wavelength) would have a half-power beamwidth of around 8 mdeg, so the goal would be errors in the region of a millidegree or less.

[1] C. Guiar, F. Lansing, R. Reynolds, and W. Merrick, "Sources of Pointing Error and Preliminary Estimates for the 64-Meter Antenna," JPL Interoffice Memorandum 3321-86-17 (internal document), Jet Propulsion Laboratory, Pasadena, California, February 28, 1986.

[2] H. McGinness, "Master Equatorial Pointing Errors at DSS 14," JPL Interoffice Memorandum 3553-84-006 (internal document), Jet Propulsion Laboratory, Pasadena, California, January 31, 1984.

II. Ring Laser Gyroscopes

Ring laser gyroscopes (RLG's) are optical devices, the operation of which is based on the Sagnac effect [3]. The

basic RLG components are given in Fig. 1. Two counter-rotating laser beams produce an interference pattern that is stationary in inertial space. Rotation of the RLG about the sensitive axis causes the interference pattern to pass over a photodetector. The output is electronically processed for zero-crossing detection and establishes one of the basic RLG error parameters: the quantization factor (Q). Two additional error sources complete the first-order error RLG model: angle random walk (q) caused by spurious emissions and bias instability (b) caused by out-of-plane mechanical reactions to the optical path-length controller.

Two stochastic error models of RLG's are shown in Figs. 2 and 3. These differ in the manner in which bias instability is modeled. In the ramp model (Fig. 2), instability is modeled as a random initial constant. At the beginning of each DSN tracking mode, a new random constant is assumed to initialize the rate integrator, thus producing a random ramp in position. This model is not useful when the bias instability changes significantly during the tracking mode (nominally 10 hr). When it is necessary to model a nonconstant bias instability, the exponential model (Fig. 3) is used. The RLG error statistics can be computed from the assumed form of the models.

Neglecting for the moment the quantization error Q, the sensor-limited performance can be computed in terms of the output variance σ_θ^2. Define an operator E[•] to be the statistical expectation of a random process. The output variance of the error models, assuming zero-mean disturbances, is $\mathrm{E}[\theta(t)\theta(t)]$. Evaluation of the statistics of Fig. 2 yields (see Appendix)

$$\sigma_\theta^2(t) = q^2 t + b^2 t^2 \tag{1}$$

The statistics of the model of Fig. 3 are also given in the Appendix as Eq. (A-2). In the following section, a method of identifying the strength of RLG error sources from recorded test data is given.

III. Allen Variance

Allen [4] developed a postprocessing technique to characterize the strength of noise terms in error models. The Allen Variance (AV) measure is defined as:

$$\sigma_{\theta_{\mathrm{AV}}}^2 = \frac{1}{2\tau^2}\mathrm{E}[(\theta_{k+2m} - 2\theta_{k+m} + \theta_k)^2] \tag{2}$$

where

$$\theta_k = \int^{k\tau_0} \dot{\theta}(t')dt' \tag{3}$$

where τ_0 is the sampling time and $\tau = m\tau_0$ is m samples. Typically, the AV assumes power-law spectral densities (PSD's) as uncorrelated error sources in angle rate:

$$s_{\dot{\theta}} = \sum_{\alpha=-2}^{\alpha=+2} h_\alpha f^\alpha \tag{4}$$

For RLG's, two error sources dominate and h_α is required to be nonzero only for $\alpha = 0$ (angle random walk) and $\alpha = -1$ (bias instability). The addition of the quantization noise PSD given by Papoulis [5] allows explicit computation of Eq. (2). The result for the noise-equivalent rate is

$$\sigma_{\dot{\theta}_{\mathrm{AV}}}^2(\tau) = 2(\log_e 2)b^2 + \frac{q^2}{\tau} + \frac{Q^2}{4\tau^2} \tag{5}$$

In terms of the noise-equivalent angle, Eq. (5) becomes

$$\sigma_{\theta_{\mathrm{AV}}}^2(\tau) = 2(\log_e 2)b^2\tau^2 + q^2\tau + \frac{Q^2}{4} \tag{6}$$

Thus the strength of noise sources is obtained by plotting the AV on a log–log plot and identifying each noise source by the slope.

Because Eq. (2) is the ensemble average over large numbers of identical experiments, practical methods of computing the AV from long-time series data on an individual RLG have been developed [6,7]. A practical approximation to the AV from N angle measurements is

$$\hat{\sigma}_{\theta_{\mathrm{AV}}}^2 = \frac{1}{2\tau^2(N-2m)} \sum_{k=1}^{N-2m} (\theta_{k+2m} - 2\theta_{k+m} + \theta_k)^2 \tag{7}$$

where N is the number of original time samples of length τ_0 and m is a parameter designating the size of the averaging interval (i.e., $\tau = m\tau_0$). The results of system-level (i. e., the sensors are installed in a mechanical subassembly, which is in turn installed into the inertial instrument) AV analyses on three laboratory RLG models[3] are given

[3] *Final Report, RL-34 Ring Laser Gyro Laboratory Evaluation for the Deep Space Network Antenna Application*, JPL Contract No. 959072 (internal document), Jet Propulsion Laboratory, Pasadena, California, November 28, 1991.

in Table 1 and arranged from best to worse. As can be seen, the best A-gyro is approximately twice as good as the C-gyro and represents improvement over several years of RLG development. These particular gyros were used in the pointing tests in Section IV. Simulation of RLG's is obtained by utilization of the noise parameters of Table 1 in the RLG error model in Fig. 3. These results are given in Fig. 4. Actual RLG error data from laboratory tests[4] are shown in Fig. 5 and verify the stochastic modeling.

IV. High-Inheritance Instrumentation

The instrument evaluated is a navigator, and as such possesses more processing capability than is actually needed in this application. The instrument computes attitude coordinates with respect to a local geographic frame (i.e., elevation, azimuth, and roll), latitude, longitude, and altitude. Azimuth and elevation only are required for DSN pointing applications. The instrument consists of a triad of RLG's, a triad of accelerometers, a sensor mounting subassembly, and processing electronics. A functional block diagram of the instrument is shown in Fig. 6. In this section, laboratory instrument test results are given for an existing navigator unit in initialization and tracking modes.

A. Laboratory Initialization Tests

Initialization is the process of determining the initial azimuth (heading) in the level geographic plane. Figure 7 defines the geographical coordinate system, which is referenced to geographic latitude vector and north. In practice, the local level plane is found by zeroing the x and y instrument accelerometers. Basically, the x and y gyro outputs are averaged until the bias instability (b) limit is reached, as shown in Eq. 5. The azimuth is found from

$$\tan^{-1}\left(\frac{g_y}{g_x}\right) = \alpha \tag{8}$$

where g_x and g_y are the averaged RLG outputs after subtraction of the Earth spin-vector projection in the level plane. This process is referred to as gyrocompassing.

The initialization tests were conducted on a Contraves 51C rate table with an air-bearing table. On top of this table was an Ultradex table for elevation adjustment. The Contraves table is installed on an isolation pad to attenuate any building coupling. An external precision metrology system provided system calibration in azimuth and elevation. Twenty-two gyrocompassing tests were conducted at nine different azimuths. The time required to reach the bias instability floor ranged from 2 to 6.25 hr. The results of laboratory initialization tests are given in Fig. 8. Summarizing, the average azimuth error over 22 tests was 0.86 mdeg.

B. Laboratory Tracking Tests

Twelve pseudo-tracking performance tests were conducted. The tests consisted of locking the Contraves and Ultradex tables on the precision pier and identifying as pointing errors all gyro outputs except those from Earth-spin components. Each test was run for 10 hr. The results are given in Table 2 and shown as an RMS error. The RMS error is the time averaged over 10 hr. The average RMS tracking error over the 10-hr interval was 3.83 mdeg.

C. Simulated Tracking Tests

To test improvements to the instrument, a simulation was coded in MatLab to emulate the instrument. A typical simulated tracking error trajectory is given in Fig. 9, which shows an end-of-track error of approximately 3 mdeg. The first simulated improvement is to change-out the lower performance gyros (B- and C-gyros in Table 1). A triad of "A" model RLG's will be used. Additionally, the scale factor Q can be reduced by a factor of 8 to reflect new threshholding electronics that are now available. With these changes, the simulated instrument tracking performance is shown in Fig. 10, which, when compared with Fig. 7, shows a performance improvement of 40 percent. The sensor-limited instrument performance confirmed analytically from Eq. (1) is 1.42 mdeg.

Thus, higher performance RLG's will significantly improve instrument performance. A search located RLG's with the following noise parameters: $q = 1.9 \times 10^{-4}$ (deg/root-hr) and $b = 4.0 \times 10^{-5}$ (deg/hr). Simulation results show that the error at the end of 10-hr tracks is less than 1 mdeg (Fig. 11).

V. Conclusion

The feasibility of utilizing inertial-sensor high-inheritance instrumentation for DSN large-structure antenna pointing was established. What was not accomplished includes

(1) Upgrade of the simulation to include accelerometer error models and Kalman filtering. In most applications, the instrument Kalman filter is run only during gyrocompassing because the instrument velocity

[4] *Final Report, RL-34 Ring Laser Gyro Evaluation for the Deep Space Network Antenna Application*, op. cit.

is known to be zero. In the DSN application, because the tracking rates are slow and nominally known, covariance improvement may be obtained by running the filter during tracks.

(2) Analysis to establish the optimum mounting location. The instrument must be mounted at a location, nominally on the rear primary reflector, that is highly correlated with the antenna pointing direction.

(3) Instrument modeling and filtering improvements. The DSN disturbance input/output modeling has not yet been incorporated into the simulation.

(4) Instrument field tests to validate the pointing error budget.

References

[1] C. Broxmeyer, *Inertial Navigation Systems*, New York: McGraw-Hill Book Company, 1964.

[2] *Advances in Inertial Navigation Systems and Components*, AGARD-AG-254, Chapter 7, pp. 7-1–7-37, available from NTIS, Springfield, Virginia, April 1981.

[3] W. W. Chow, V. E. Sanders, W. Schleich, and M. O. Scully, "The Ring Laser Gyro," *Reviews of Modern Physics*, vol. 57, no. 1, pp. 61–104, January 1985.

[4] D. Allan, P. Kartaschoff, J. Vanier, J. Vig, G. M. R. Winkler, and N. G. Yannoni, "Standard Terminology for Fundamental Frequency and Time Metrology," *Proceedings of the IEEE 42nd Annual Frequency Control Symposium*, Baltimore, Maryland, pp. 419–425, 1988.

[5] A. Papoulis, *Probability, Random Variables, and Stochastic Processes*, New York: McGraw-Hill, 1965.

[6] D. Sargent and B. O. Wyman, "Extraction of Stability Statistics From Integrated Rate Data," paper 80-1728, *Proceedings of the Guidance and Control Conference*, American Institute of Aeronautics and Astronautics, Danvers, Massachusetts, pp. 88–94, 1980.

[7] A. D. King, *Characterisation of Gyro In-Run Drift*, Edinburgh, Scotland: Ferranti Defence Systems Ltd., Navigation Systems Department, 1971.

Table 1. Allen Variance analysis on three RLG models.

Gyro models	Quantization (Q), mdeg/pulse	Angle random walk (q), mdeg/root-hr	Bias instability (b), mdeg/hr
A	0.106	0.30	0.16
B	0.106	0.42	0.20
C	0.106	0.59	0.40

Table 2. Laboratory tracking test results.

RMS azimuth error, mdeg	RMS elevation error, mdeg	RMS pointing, mdeg	Description
3.6111	0.8056	3.6667	El = 0 deg[a]
4.8889	1.2222	4.9444	El = 0 deg
5.5833	0.4722	5.6111	El = 0 deg[b]
3.4444	1.1111	3.5556	El = 0 deg
5.1944	1.0000	5.2222	El = 0 deg
3.7778	0.5833	3.7778	El = 0 deg
			Recalibration[c]
3.0000	0.7500	3.1111	El = 0 deg
1.2778	0.4722	1.3611	El = 0 deg[d]
3.1111	1.0556	3.2778	El = 60 deg
4.7778	0.8333	4.8333	El = 60 deg
2.8889	1.0278	3.0556	El = 60 deg
3.5833	1.0833	3.7500	El = 60 deg
—	—	3.8333	Average pointing over 12 tests
—	—	3.2283	Average after recalibration

[a] Typical.

[b] Worst case.

[c] One month from previous calibration.

[d] Best case.

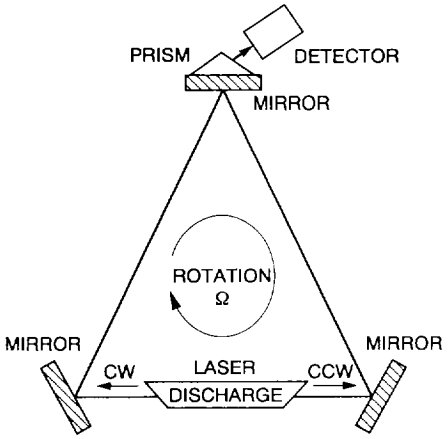

READOUT IS IN COUNTS/SEC
SCALE FACTOR = $(\lambda L/4A)$

SAGNAC EFFECT

COUNTER-PROPAGATING BEAMS TRAVEL IDENTICAL PATHS

ROTATION OF GYRO PRODUCES A PHASE DIFFERENCE OF THE TWO BEAMS

PHASE CHANGE = $\Delta\phi = (8\pi A/\lambda c)\Omega$

WHERE A = ENCLOSED AREA
λ = LASER WAVELENGTH
Ω = GYRO ROTATION RATE
c = SPEED OF LIGHT

PROPAGATION TIME ALONG CLOSED PATH OF LENGTH L IS $\tau = L/c$

RATE OF PHASE CHANGE = $2\pi\Delta f = \Delta\phi/\tau$

THUS, $2\pi\,\Delta f = \Delta\phi^*(c/L) = 2\pi\,(4A/\lambda L)\,\Omega$

WHERE Δf = OUTPUT FREQUENCY

TYPICAL SCALE FACTOR = 1.5 arcsec/count

(FOR CIRCULAR PATH OF RADIUS R, SCALE FACTOR = $\lambda/2R$)

Fig. 1. Ring laser gyro component diagram and operating principal.

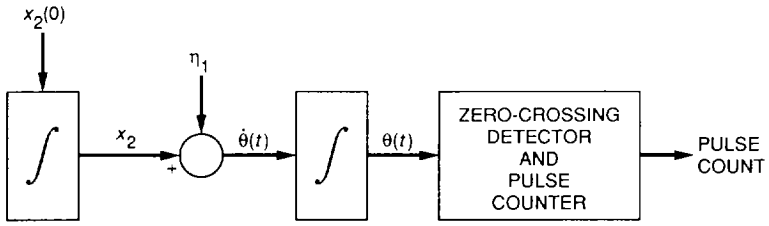

Fig. 2. Stochastic RLG model with ramp bias instability.

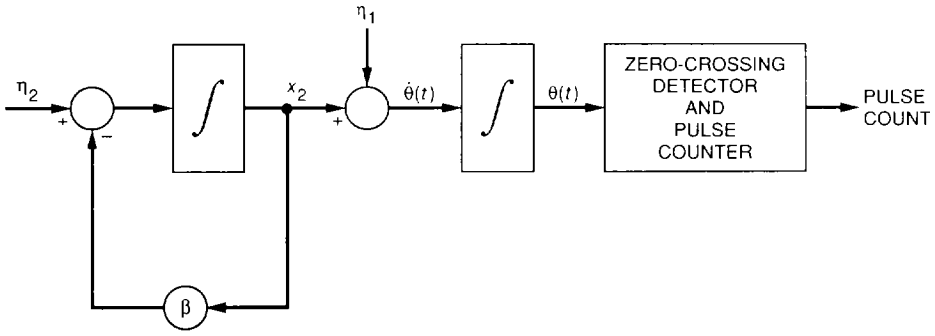

Fig. 3. Stochastic RLG model with exponential bias instability.

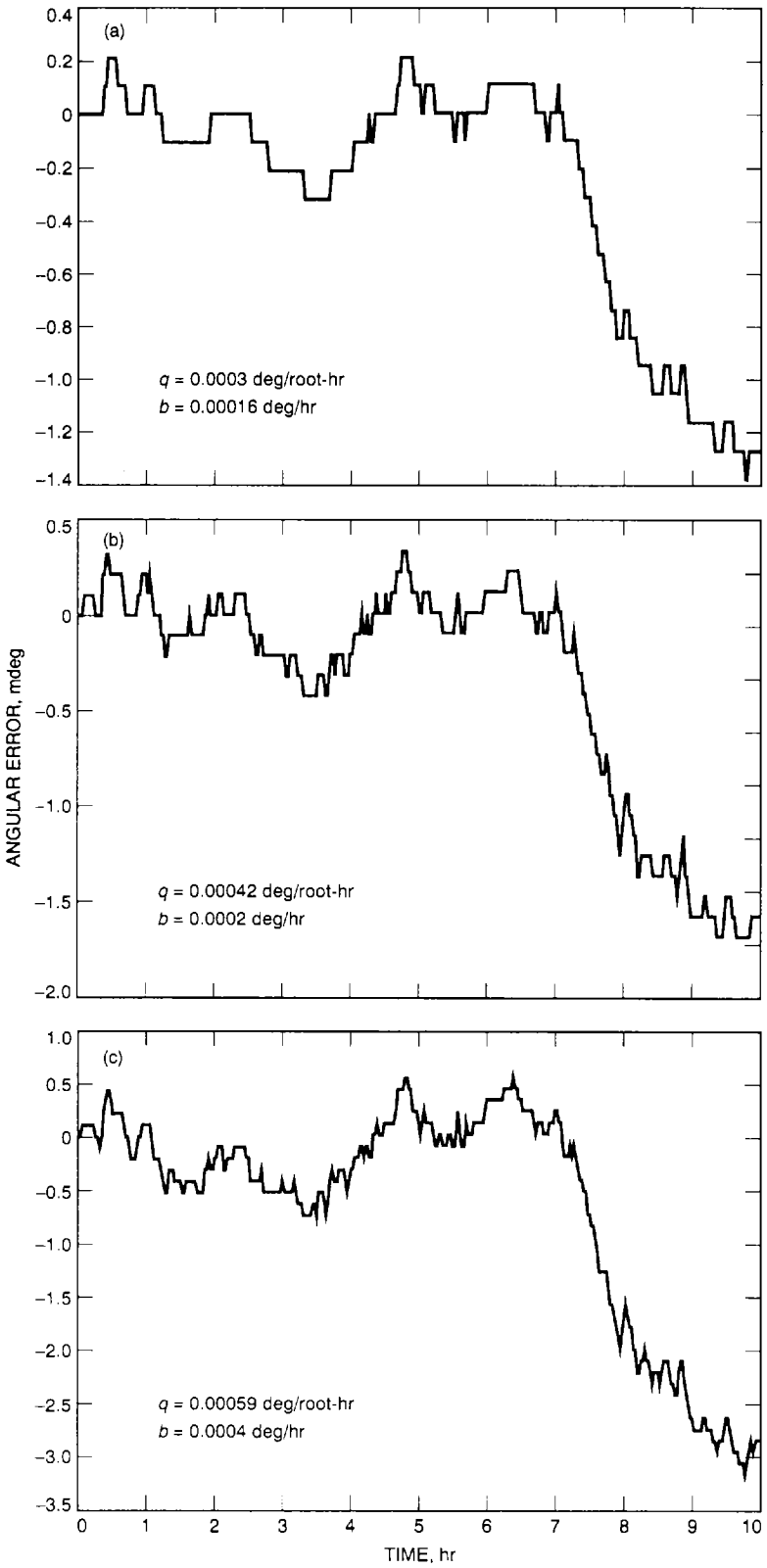

Fig. 4. Simulated gyro error with exponential bias instability: (a) A-gyro; (b) B-gyro; and (c) C-gyro.

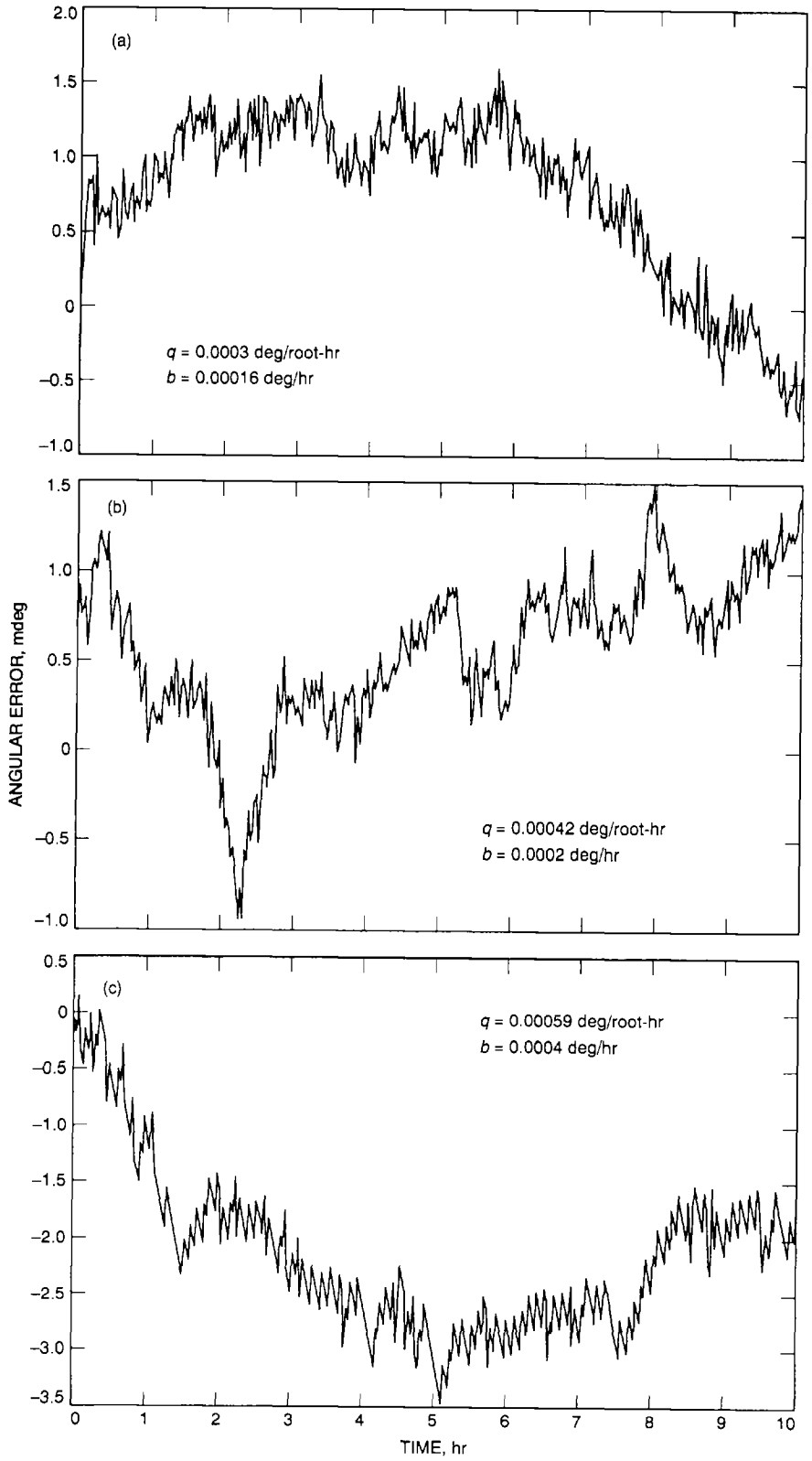

Fig. 5. Actual gyro laboratory test error: (a) A-gyro; (b) B-gyro; and (c) C-gyro.

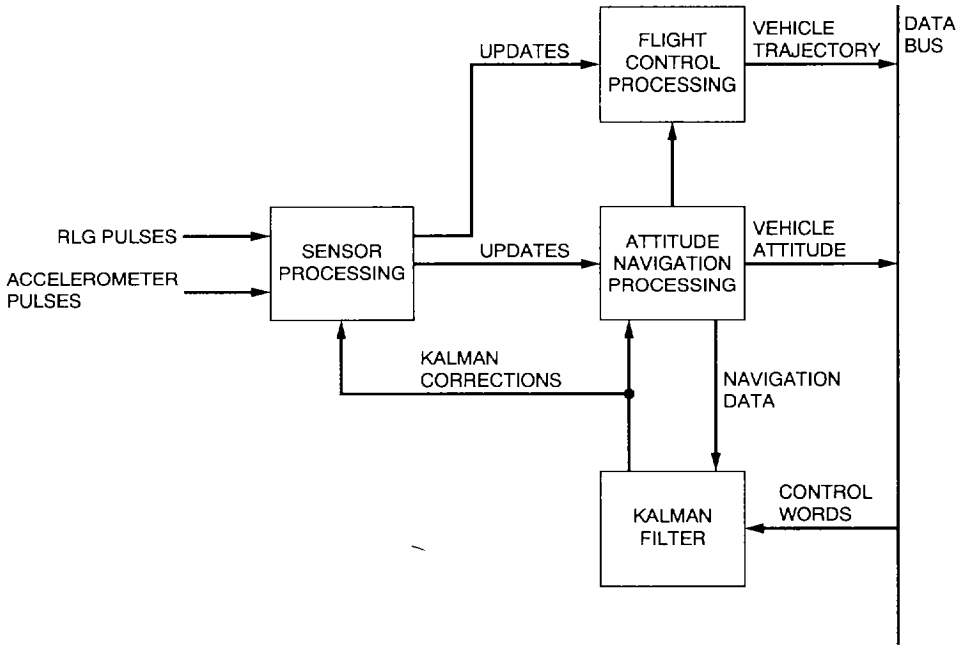

Fig. 6. Functional block diagram of inertial navigator.

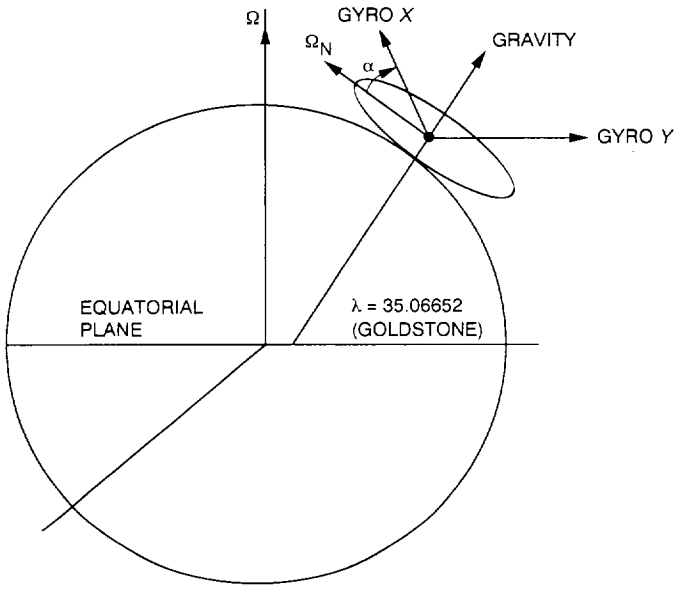

Fig. 7. Initialization frame.

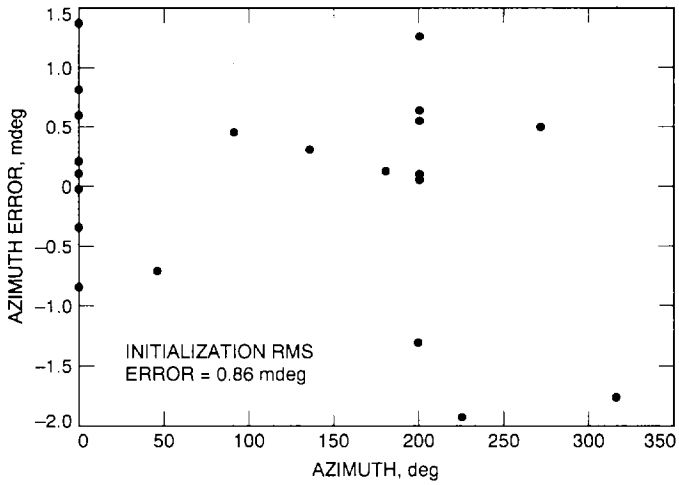

Fig. 8. Initialization-mode laboratory test results.

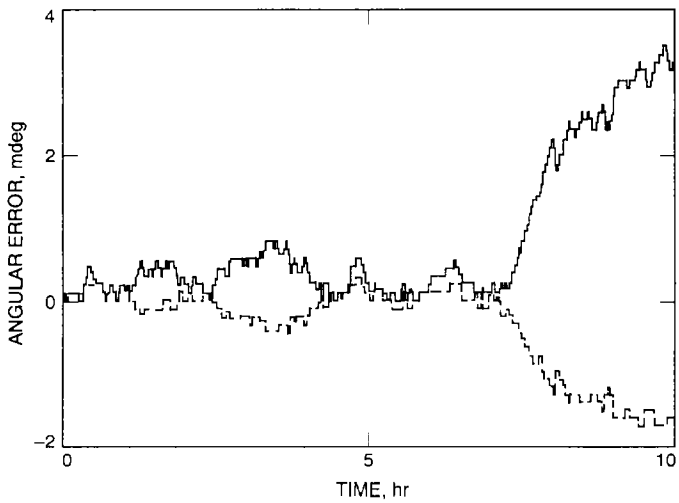

Fig. 9. Simulated system-level tracking error.

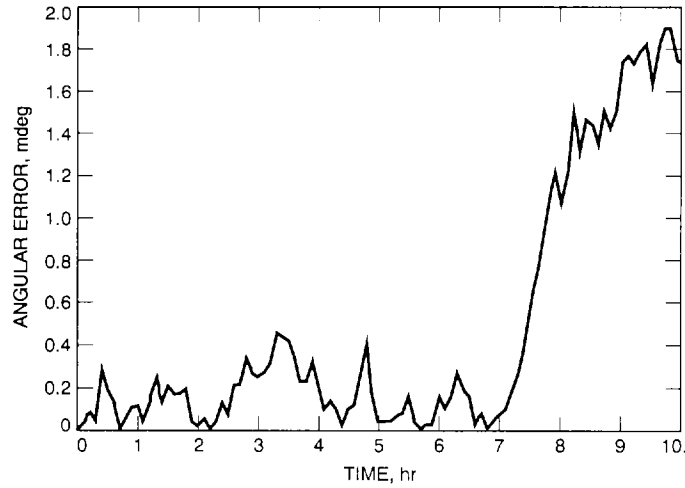

Fig. 10. Simulated tracking improvement with all A-gyros.

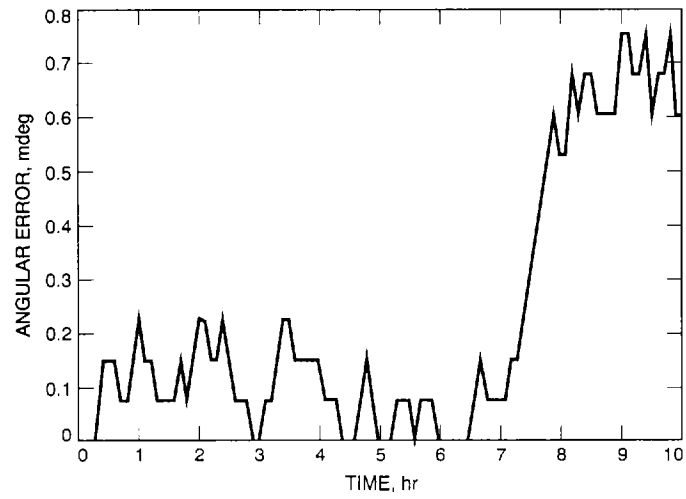

Fig. 11. Simulated tracking error with best performing gyros.

Appendix

The state equations of Fig. 2 are

$$\dot{\vec{x}} = \begin{bmatrix} 0 & 1 \\ 0 & 0 \end{bmatrix} \vec{x} + \begin{bmatrix} 1 \\ 0 \end{bmatrix} \eta_1$$

where $[x_1, x_2]^T$ *and* $x_1 = \theta$. Then

$$\dot{\vec{x}} = A\vec{x} + G\vec{\eta}$$

Let

$$\mathrm{E}\left[\vec{\eta}\vec{\eta}^T\right] = \sigma_{\eta_1}^2 \delta(\xi) \quad \text{(scalar)}$$

where η is a zero-mean white-noise process. Without tracking aids (fixes), the covariance of $\theta(t)$ increases in time. The linear covariance equation is

$$\dot{P} = AP + PA^T + GQG^T$$

and from previous notation,

$$Q = \begin{pmatrix} \sigma_{\eta_1}^2 & 0 \\ 0 & 0 \end{pmatrix}$$

Solving by assuming $\mathrm{E}[x_2(0)\theta(0)] = \mathrm{E}[\theta(0)\theta(0)] = \mathrm{E}[x_2(0)\eta_1(t)] = 0$,

$$\sigma_\theta^2(t) = E\left[x_2^2(0)\right] t^2 + \sigma_{\eta_1}^2 t \qquad \text{(A-1)}$$

In deriving Eq. (A-1), it is also understood that $x_2(0)$ and $\theta(0)$ are zero-mean.

The state equations of Fig. 3 are

$$\dot{\vec{x}} = \begin{bmatrix} 0 & 1 \\ 0 & -\beta \end{bmatrix} \vec{x} + \begin{bmatrix} 1 & 0 \\ 0 & 1 \end{bmatrix} \vec{\eta}$$

As before, let

$$\mathrm{E}\left[\vec{\eta}\vec{\eta}^T\right] = \begin{pmatrix} \sigma_{\eta_1}^2 & 0 \\ 0 & \sigma_{\eta_2}^2 \end{pmatrix} \delta(\xi)$$

be zero-mean and uncorrelated random processes and $x_2(0) = \theta(0) = 0$. Writing and solving the differential equations from the linear covariance equation yields

$$\sigma_\theta^2(t) = \sigma_{\eta_1}^2 t + \sigma_{\eta_2}^2 t + \left(\frac{\sigma_{\eta_2}^2}{2\beta^3}\right)\left(1 - e^{-2\beta t}\right)$$

$$+ \left(\frac{2\sigma_{\eta_2}^2}{\beta^3}\right)\left(e^{-\beta t} - 1\right) \qquad \text{(A-2)}$$

The correlation time β is computed, as a rule of thumb, to allow the gyro output uncertainty to reach the variance given by Eq. (A-1) at the end of a track.